Coarse analysis of collective motion with different communication mechanisms

Allison Kolpas [a,*], Jeff Moehlis [b], Thomas A. Frewen [c], Ioannis G. Kevrekidis [c,d]

[a] Department of Mathematics, University of California, Santa Barbara, CA 93106, USA
[b] Department of Mechanical Engineering, University of California, Santa Barbara, CA 93106, USA
[c] Department of Chemical Engineering, Princeton University, Princeton, NJ 08544, USA
[d] Program in Applied and Computational Mathematics, Princeton University, Princeton, NJ 08544, USA

ARTICLE INFO

ABSTRACT

We study the effects of a signalling constraint on an individual-based model of self-organizing group formation using a coarse analysis framework. This involves using an automated data-driven technique which defines a diffusion process on the graph of a sample dataset formed from a representative stationary simulation. The eigenvectors of the graph Laplacian are used to construct 'diffusion-map' coordinates which provide a geometrically meaningful low-dimensional representation of the dataset. We show that, for the parameter regime studied, the second principal eigenvector provides a sufficient representation of the dataset and use it as a coarse observable. This allows the computation of coarse bifurcation diagrams, which are used to compare the effects of the signalling constraint on the population-level behavior of the model.

© 2008 Elsevier Inc. All rights reserved.

1. Introduction

Animal groups, such as schools of fish, flocks of birds, swarms of locusts, and herds of wildebeest, often display collective motion [1–5]. Such groups may exhibit a variety of behaviors including swarming about a food source, milling around a central location, or migrating over large distances in aligned groups. These collective behaviors are often advantageous to groups, allowing them to increase their harvesting efficiency [3,6], better follow migration routes [7], improve their aerodynamic efficiency [8,9], and avoid predation [10,11]. In such self-organized groups, there is no leader directing the motion of the individual members. Instead, the local interactions of the individual group members with their nearby neighbors gives rise to the collective dynamics [1].

A single animal group may display different collective behaviors at different times [12]. For the one-dimensional individual-based schooling model studied in [13], it was shown that stochasticity in individual decisions can be responsible for switching between co-existing collective motion states, corresponding to a 'stationary state', in which the dynamics are driven by repulsion with the school remaining approximately stationary in time, and a 'mobile state', in which the school is aligned and travels in the positive or negative direction.

In the schooling model in [13], it was assumed that individuals are able to communicate with *all* neighbors within their behavioral

zones, regardless of their relative position/orientation (i.e., irrespective of whether they are ahead or behind or facing towards or away). For many animal groups, however, it is realistic to assume that individuals may only receive some signals unidirectionally [14–16]. This might be due to many factors including their physiology, behavioral preferences, or environmental conditions [17,18]. Most organisms, for example, have a limited field of vision, and neighbors in their 'blind spot' are visually undetectable. In the presence of predators, birds may use directional sound cues to prevent receivers other than the addressee from obtaining information [16]. In [19], different animal communication mechanisms were explored for a one-dimensional hyperbolic partial differential equation model for group formation. Here we compare the effects of a change in the communication protocol on the individual-based schooling model. More specifically, we consider the case where individuals receive repulsion and attraction signals omnidirectionally but orient only with those facing towards them (this is called mechanism M1 in [19]). In this paper, we demonstrate quantitatively how this signalling constraint affects the properties of collective motion.

The average distance to the nearest neighbor was used as a coarse variable in [13] to characterize the collective behavior of the school. This was shown to be a dynamically meaningful observable through computational experiments testing different candidate observables. However, as discussed in [13], the value of this coarse variable can depend on details of the positions of the individuals which do not affect the dynamics. This is a consequence of the fact that the dynamics of each individual are determined only by the occupancies of each of its behavioral zones (by other individuals): details of the positions of individuals within these

* Corresponding author. Tel.: +1 805 450 1048.
E-mail addresses: allie@math.ucsb.edu (A. Kolpas), moehlis@engineering.ucsb.edu (J. Moehlis), tfrewen@Princeton.edu (T.A. Frewen), yannis@Princeton.edu (I.G. Kevrekidis).

zones are not important. This may be viewed as a 'neutral stability' property of solutions to the model.

In the present paper, we use an automated data-driven technique for generating coordinates that correlate with the collective behavior of the school. We construct the normalized graph Laplacian by interpreting a sample simulation dataset as a graph whose connection strengths are given by a Gaussian kernel [20]. Using the framework developed in [21], we then construct 'diffusion map' coordinates from the eigenvectors of this matrix and use them to provide a geometrically meaningful lower-dimensional representation of the dataset. The advantage of using such an approach over traditional methods such as principal component analysis is that it is non-linear and preserves the local dataset geometry [22]. Further discussion on using diffusion maps as reaction coordinates for stochastic dynamical systems can be found in [23]. The diffusion map framework allows us to find a low dimensional representation of the dynamics of the schooling model. Specifically, we show that here, a single diffusion map coordinate is sufficient to characterize the dynamics. This coordinate also overcomes the 'neutral stability' issue which arose for the coarse variable used in [13]. An effective potential is computed and used to locate metastable states, their parametric dependencies, and estimate mean switching times as in [13]. Coarse bifurcation diagrams are constructed for each of the models and compared to quantify the effects of the signalling constraint on the collective dynamics. Overall, our results suggest that the diffusion map framework constitutes a promising approach for understanding collective motion for fish schooling models.

2. Schooling model

We consider a one-dimensional individual-based model for schooling with local behavioral interactions. Similar individual-based models have been studied in [13,24–28]. Groups are composed of N individuals with positions $c_i(t) \in \mathbb{R}$, unit directions $v_i(t) = \pm 1$, and constant speed $s \in \mathbb{R}$. Every time step τ, individuals simultaneously determine their direction of travel by considering neighbors within three non-overlapping behavioral zones, a zone of repulsion of radius r_r, and zones of orientation and attraction with widths Δr_o, and Δr_a, respectively; see Fig. 1.

These zones are used to define behavioral interaction rules. First, if an individual i finds other agents within its zone of repulsion Z_{r_i}, then it orients its direction away from the average relative directions of those agents. Its desired direction of travel in the next time step is given by

$$v_i(t+\tau) = - \sum_{\substack{c_j(t) \in Z_{r_i}(t) \\ i \neq j}} \frac{c_j(t) - c_i(t)}{|c_j(t) - c_i(t)|}. \tag{1}$$

This vector is normalized as $v_i(t+\tau) \to \frac{v_i(t+\tau)}{|v_i(t+\tau)|}$, assuming $v_i(t+\tau) \neq 0$. In the case that $v_i(t+\tau) = 0$, agent i maintains its previous direction of travel with $v_i(t+\tau) = v_i(t)$.

If agents are not found within individual i's zone of repulsion, then it aligns with neighbors within its zone of orientation Z_{o_i} by computing an average over their directions and that of itself. Attraction of agent i to neighbors within its zone of attraction Z_{a_i} is imposed by orienting it towards the average of their relative directions. The desired direction of agent i is then given by the sum of two terms,

$$v_i(t+\tau) = \frac{v_i(t) + \sum_{c_j(t) \in Z_{o_i}(t)} v_j(t)}{\left| v_i(t) + \sum_{c_j(t) \in Z_{o_i}(t)} v_j(t) \right|} + \frac{\sum_{c_j(t) \in Z_{a_i}(t)} \frac{c_j(t) - c_i(t)}{|c_j(t) - c_i(t)|}}{\left| \sum_{c_j(t) \in Z_{a_i}(t)} \frac{c_j(t) - c_i(t)}{|c_j(t) - c_i(t)|} \right|}. \tag{2}$$

For the *constrained* signalling model, an agent only aligns with those in its zone of orientation that are facing towards itself (i.e., moving in the direction that it is facing). In this case, the orientation summation index in (2) will change to $\{c_j(t) \in Z_{o_i}(t) | v_j(t) \frac{c_j(t) - c_i(t)}{|c_j(t) - c_i(t)|} = -1\}$. In both cases, the vector contribution from orientation and alignment is then normalized as $v_i(t+\tau) \to \frac{v_i(t+\tau)}{|v_i(t+\tau)|}$, assuming $v_i(t+\tau) \neq 0$. As before, if $v_i(t+\tau) = 0$, then agent i maintains its previous direction of travel.

Stochastic effects are incorporated into the model by changing the sign of agent i's desired direction with probability p. Finally, each agent's position is updated simultaneously using

$$c_i(t+\tau) = c_i(t) + s v_i(t+\tau)\tau. \tag{3}$$

To begin a simulation, individuals are placed in a bounded region (so that each agent initially interacts with at least one other agent) with randomized positions and directions of travel.

For the parameters studied in [13], namely $N = 100$, $s = 0.75$, $\tau = 0.1$, $r_r = 1$, $0.1 < \Delta r_o < 1.3$, $\Delta r_a = 1$, $p = 0.001$, we observe that both models, each with a different communication rule, can display two metastable collective states: a 'stationary state', in which the dynamics are driven by repulsion, and a 'mobile state', in which the school is aligned and travels in the positive or negative direction. For certain values of the parameters, the school stochastically switches between the stationary and mobile state. For the signal constrained model the mobile state only exists for higher values of Δr_o; a detailed bifurcation analysis will be performed later in the paper to quantify this more precisely.

3. Diffusion maps: data-driven detection of coarse observables

3.1. Background

For many complex biological systems, it is difficult to identify appropriate coarse variables ('observables', or 'reaction-coordinates') that correlate with the population-level behavior of the system and capture its geometric structure. In addition, often such systems have many degrees of freedom and it is useful to explore methods for reducing their dimensionality. Here we summarize a data-mining technique for obtaining a low-dimensional representation of a high-dimensional dataset [21,23,29], and show how it can be applied to find an appropriate coarse observable for our schooling models. This technique has been successfully applied to other biological models in [28,30,31].

3.2. Diffusion map theory

Suppose $\{X^{(i)}\}_{i=1}^m$ is a finite dataset with each $X^{(i)} \in \mathbb{R}^N$. A random walk may be defined on a graph based on the dataset constructed as follows. Points in the dataset correspond to nodes of a graph with connection strength given by a Gaussian kernel. (In [21], anisotropic kernels formed from renormalizing the Gaussian kernel were also explored.) Applying the graph Laplacian normalization [20] to the kernel, one may form a Markov (row stochastic) matrix M. With this framework, one can quantify the similarity between datapoints, the 'diffusion distance', by comparing the prob-

Fig. 1. Behavioral zones for the one-dimensional fish schooling model: Z_r = zone of repulsion, Z_o = zone of orientation, and Z_a = zone of attraction.

ability distributions of the end points of random walks starting at the nodes of the graph. A 'diffusion map', which maps datapoints to their eigencomponents in diffusion map space, is constructed from the first k eigenvectors of M. It was proved in [29] that diffusion distance is equal to Euclidean distance in diffusion map space. Thus, datapoints that are close together in diffusion distance are mapped to points close together in Euclidean distance in diffusion map space. In addition, if M has a spectral gap, it was shown that a $k < N$ dimensional approximation is optimal under a certain mean squared error criterion.

Asymptotic analysis has also shown that for datasets sampled from an underlying probability distribution, written in Boltzmann form as $p(x) = e^{-U(X)}$ with potential $U(X)$, in the limit that the sample size $m \to \infty$ and the standard deviation of the kernel $\sigma \to 0$, the random walk on the graph converges to a diffusion process which can be described by a Fokker-Planck equation [29]. Different normalizations of the Gaussian kernel were shown to produce different differential operators [23]. In particular, for the isotropic Gaussian kernel, the eigenvalues and eigenvectors of M are discrete approximations to the eigenvalues and eigenfunctions of the Fokker-Planck operator with potential $2U(X)$. In the case that $U(X)$ (and thus $2U(X)$) has two wells separated by a large barrier (i.e., the dataset has two well-separated clusters), then the diffusion map approach can identify a single coarse observable, the first non-trivial (second principal) eigenvector, whose components parametrize the dataset.

3.3. Diffusion map coordinates and Nyström extension

We now review the procedure for computing diffusion map coordinates for a dataset, including the use of the Nyström extension to obtain diffusion map coordinates for points outside the dataset. (See [31] for an example of this approach applied to a neural field model.) Let $\{X^{(i)} \in \mathbb{R}^N\}_{i=1}^m$ be a finite dataset with distance measure $d : \mathbb{R}^N \times \mathbb{R}^N \to \mathbb{R}$. For our model, this corresponds to snapshots of the school taken from a representative steady state simulation. Next, define the Gaussian kernel $K(X^{(i)}, X^{(j)}) = \exp\{-[d(X^{(i)}, X^{(j)})]^2/\sigma^2\}$ and its corresponding matrix representation $K_{i,j} = K(X^{(i)}, X^{(j)})$. Let $D_{i,i} = \sum_{j=1}^m K_{i,j}$ be the diagonal matrix formed from the row sums of K. Then, the Markov (row stochastic) matrix $M = D^{-1}K$ defines a random walk on a graph whose nodes correspond to the points in the dataset. The entries $M_{i,j}$ can be interpreted as representing the probability of transition from $X^{(i)}$ to $X^{(j)}$ in the time $\Delta t = \sigma$ [29].

Define the symmetric matrix $M_s = D^{1/2}MD^{-1/2}$. Note that M is related to M_s through a similarity transformation, so they share the same eigenvalues. Since M_s is symmetric, it is diagonalizable, and its eigenvectors $\{\Psi_j\}_{j=1}^m$ form an orthonormal basis of $\mathbb{R}^m$. Let $\{\lambda_j\}_{j=1}^m$ be the corresponding (real) eigenvalues of M_s and M. Then the eigenvectors $\{\Phi_j\}_{j=1}^m$ of M are related to those of M_s by the relation $\Phi_j = D^{-1/2}\Psi_j$. For σ large enough, all points are connected (M is strictly positive) and it follows from the Perron–Frobenius Theorem [33] that $\lambda_1 = 1$ is a unique eigenvalue with corresponding eigenvector $\Phi_1 = [1, 1, \ldots]$ and $1 > \lambda_2 \geqslant \lambda_3 \geqslant \lambda_4 \geqslant \ldots \lambda_m \geqslant 0$. The diffusion map $f : \mathbb{R}^N \to \mathbb{R}^k$ is defined as

$$f : X^{(i)} \to \left(\Phi_2^{(i)}, \Phi_3^{(i)}, \ldots \Phi_{k+1}^{(i)}\right), \tag{4}$$

where an appropriate k is chosen based on the spectral gap. Here k is the number of non-trivial eigenvalues clustered near one with all additional eigenvalues close to zero. The notation $\Phi_k^{(i)}$ represents the ith component of the kth eigenvector. In practice, we compute the eigenvalues and eigenvectors of M_s and then use the relation $\Phi_j = D^{-1/2}\Psi_j$ to find the eigenvectors of M.

We now discuss how to compute the diffusion map coordinates for points outside of our dataset. By definition, the eigenvectors Ψ_j of M_s satisfy the following equation

$$\Psi_j^{(k)} = \frac{1}{\lambda_j} \sum_{i=1}^m M_s(X^{(k)}, X^{(i)})\Psi_j^{(i)}. \tag{5}$$

Here $M_s = D^{-1/2}KD^{-1/2}$, so that the component

$$(M_s)_{k,i} \equiv M_s(X^{(k)}, X^{(i)}) = \frac{K(X^{(k)}, X^{(i)})}{\sqrt{\sum_{j=1}^m K(X^{(k)}, X^{(j)}) \sum_{j=1}^m K(X^{(i)}, X^{(j)})}}. \tag{6}$$

The eigenvectors Φ_j of M satisfy

$$\Phi_j^{(k)} = \frac{1}{\sqrt{D_{k,k}}} \Psi_j^{(k)} = \frac{1}{\sqrt{\sum_{j=1}^m K(X^{(k)}, X^{(j)})}} \Psi_j^{(k)}. \tag{7}$$

We can extend these formulas for a point $X^{(\text{new})}$ outside the dataset using the Nyström extension [34] as follows:

$$\Psi_j^{(\text{new})} = \frac{1}{\lambda_j} \sum_{i=1}^m \widetilde{M}_s(X^{(\text{new})}, X^{(i)})\Psi_j^{(i)}, \tag{8}$$

where

$$\widetilde{M}_s(X^{(\text{new})}, X^{(i)}) = \frac{K(X^{(\text{new})}, X^{(i)})}{\sqrt{\sum_{j=1}^m K(X^{(\text{new})}, X^{(j)}) \sum_{j=1}^m K(X^{(i)}, X^{(j)})}} \tag{9}$$

$$= \frac{1}{m} \frac{K(X^{(\text{new})}, X^{(i)})}{\sqrt{\langle K(X^{(\text{new})}, X^{(j)})\rangle \langle K(X^{(i)}, X^{(j)})\rangle}}, \tag{10}$$

and $\langle \cdot \rangle$ denotes expectation over all elements of the dataset. New datapoints in the Φ coordinates are related by the equation

$$\Phi_j^{(\text{new})} = \frac{1}{\sqrt{\sum_{j=1}^m K(X^{(\text{new})}, X^{(j)})}} \Psi_j^{(\text{new})}. \tag{11}$$

An eigendecomposition is typically performed using a sample database and the Nyström extension is used to efficiently compute the diffusion map coordinates for points outside of the database. It is worth noting that the Nyström extension can be quite successful in *interpolating* new points, but can quickly and spectacularly fail when extrapolating beyond the original database. A discussion of this can be found in [35].

4. Distance measure for the schooling model

In order to form a Markov matrix whose leading eigenvectors provide a reduced set of coarse observables for our dataset, we must first define a distance measure between schools. We choose the one described below which leads to useful diffusion map coordinates.

Let N be the size of a school and $d_{i,j}$ denote the Euclidean distance between fish i and j. In the following, we will assume that members of a given school have been sorted by position in increasing order from left to right. Two schools are considered 'close' in distance if they are composed of members exhibiting the same behavioral responses at the same ordering index within the school (modulo the left-right reflection symmetry). To account for the the fact that the behavioral zones elicit the same response for a range of distances, we first replace distances $d_{i,i+1}$, $i = 1, \ldots N - 1$ between subsequent individuals as follows:

$$d_{i,i+1} \to \begin{cases} r_r, & d_{i,i+1} \leqslant r_r \\ r_o, & r_r < d_{i,i+1} \leqslant r_o \\ r_a, & r_o < d_{i,i+1} \leqslant r_a \\ r_a + \delta, & d_{i,i+1} > r_a \end{cases}$$

That is, immediate neighbors within the repulsion (resp., orientation, attraction) zone are moved a fixed distance r_r (resp., r_o, r_a) apart. Agents that are spaced a distance $d_{i,i+1} > r_a$ apart, who do

not feel any social forces, are moved a fixed distance $r_a + \delta$ from one another. The precise value of δ is not important; in the following we take $\delta = r_r$. After replacing distances, the schools are shifted so that the center of mass lies at the origin.

After this rearrangement, let x_i and y_i, $i = 1, \ldots N$, be the positions of individuals in schools X and Y, respectively. The distance $d(X, Y)$ between schools X and Y is defined as

$$d(X, Y) = \min(d_1, d_2),$$

where

$$d_1 = \sqrt{\sum_{i=1}^{N}(x_i - y_i)^2}, \qquad d_2 = \sqrt{\sum_{i=1}^{N}(x_i - (-y_{N+1-i}))^2}.$$

Here d_1 and d_2 are the Euclidean distances between vectors in $\mathbb{R}^N$ whose components are the (one-dimensional) coordinates of the sorted positions of the individuals within the school. Note that we take $\min(d_1, d_2)$ to take into account the reflection symmetry.

5. Diffusion map coordinates for the schooling model

Starting with this measure of distance, we can form a Markov matrix from long-time stationary simulation data of the model and compute diffusion map coordinates. First we show some results from a dataset created by sampling every 8 time units a 10^4 step run (after initial transients have passed) of the original fish schooling model with $N = 100$, $r_r = 1$, $\Delta r_0 = 0.6$, $\Delta r_a = 1$, and $\sigma = 40$ for the diffusion kernel. Note that the Gaussian kernel acts as a non-linear transformation on distances between points in the dataset. The variance of the kernel, σ, should be chosen so that points close by (in the same potential well) have a value close to one, while points that are far away (in different wells) have a value close to zero and thus not directly connected to the graph of the dataset. For the distance measure chosen in Section 4, 'far away' is on the order of 90 units, while 'close by' is on the order of 5 units. This narrows the range of possible values for σ. In practice, different values of σ were tested, and the spectral gap was used as an

indicator of an appropriate choice. See Appendix for an example which compares the effects of varying σ and relates the diffusion map procedure to principal component analysis.

Fig. 2 shows a space-time plot of the school as well as its low-dimensional representation in terms of the second principal eigenvector $\Phi_2^{(i)}$. In Fig. 3 we show that the data collapse on an approximately one-dimensional manifold (projected here on the $(\Phi_2^{(i)}, \Phi_3^{(i)})$ plane). Simulation points in the $(\Phi_2^{(i)}, \Phi_3^{(i)})$ coordinates are colored according to their associated value of the empirical coordinate used in [13]:
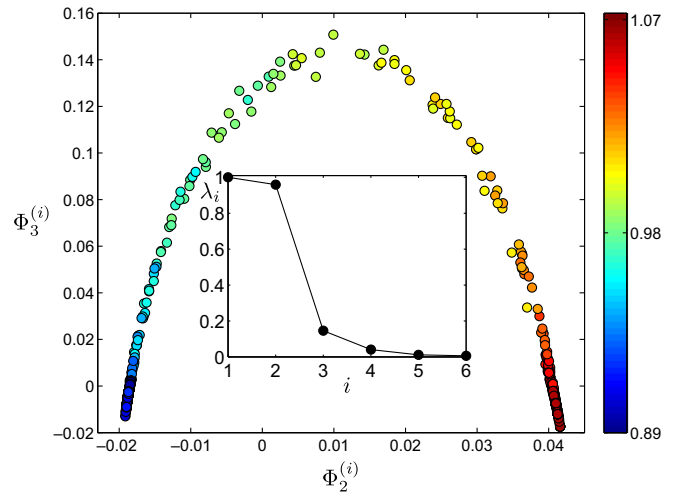

Fig. 3. Plot of the data in the plane of the first two non-trivial eigenvectors $(\Phi_2^{(i)}, \Phi_3^{(i)})$ constructed from the simulation dataset. Simulation points in the diffusion map coordinates are colored according to their associated value of the coordinate A, average distance to nearest neighbor. Inset: Plot of the first few eigenvalues. Since there is a spectral gap, we are justified in keeping $\Phi_2^{(i)}$ as a single observable for the system.
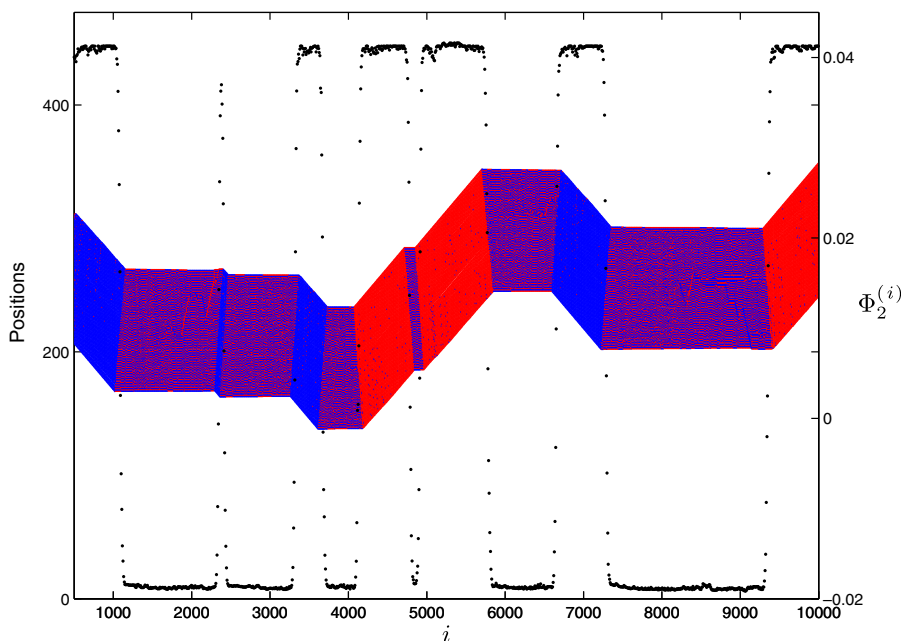

Fig. 2. Positions of $N = 100$ agents (after transient) for a 10^4 step run of the original schooling model with parameters $s = 0.75$, $\tau = 0.1$, $r_r = 1$, $\Delta r_0 = 0.6$, $\Delta r_a = 1.0$, $p = 0.001$; red (resp., blue) indicates motion of an agent in the positive (resp., negative) direction. The black dots indicate the corresponding diffusion map coordinate representation. (For interpretation of the references to color in this figure legend, the reader is referred to the web version of this paper.)

$$A(t) = \frac{1}{N} \sum_{i=1}^{N} \min_{j \neq i} |c_j(t) - c_i(t)|, \tag{12}$$

the average distance between nearest neighbors. When A is large (red), the school is in the 'mobile' state, and when A is small (blue), the school is in the 'stationary' state. Since the manifold is approximately one-dimensional and there is a large gap in the eigenvalue spectrum, we appear justified in keeping the first non-trivial eigenvector as our coarse observable. The first panel of Fig. 4 shows the dataset in the two coordinates $\Phi_2^{(i)}$ and A.

The second panel of Fig. 4 shows why the observable A is less useful than the diffusion map coordinates. This dataset was obtained by running a 10^4 step simulation of the schooling model with the same parameters as above but with a slightly different initial population density. Like the previous dataset, the school is transitioning between the stationary and mobile state, however A takes values in the range [0.98, 1.13] instead of [0.92, 1.07]. This is a consequence of the model, which specifies rules of motion based on occupancies of zones, allowing the school to exhibit the same dynamics at a range of distances between neighbors. Our

new distance measure avoids this problem by systematically replacing the range of distances which yield the same response in the model by a single distance. As can be seen from Fig. 4, the diffusion map coordinate $\Phi_2^{(i)}$, obtained on this new dataset by using the Nyström extension, gives values in the same range as the previous dataset.

In some cases, a school may fragment into subgroups displaying the same or different dynamics. As in [13], such fragmented states will not be included in the coarse analysis of the dynamics of the schooling models. Clearly, multiple coordinates are necessary to successfully describe fragmentation and will be the subject of future work.

6. Estimating the effective potential and mean residence times

We may construct an effective potential in terms of the coarse observable X (in our case Φ_2) from long-time simulation data in one of two ways. The simplest approach is to form a probability distribution function $P(X)$ from long-time simulation statistics and then use the relation $U(X) = -\log(P(X)) + \text{const.}$ This method
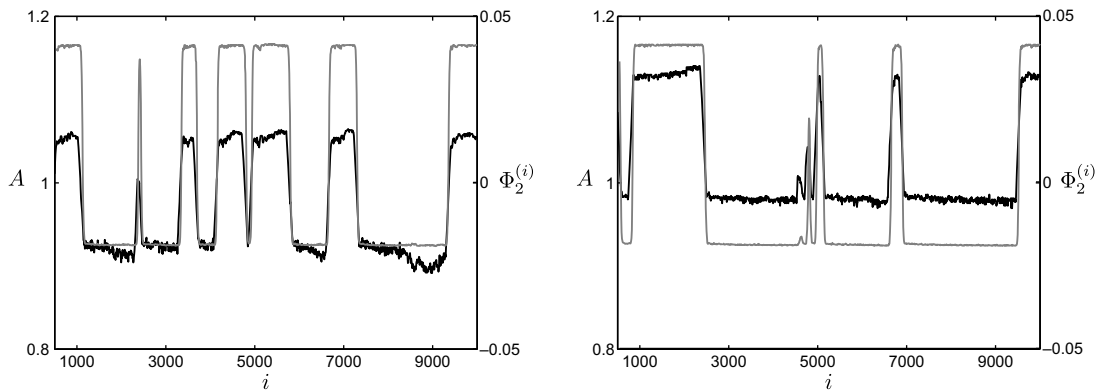

Fig. 4. Left Panel: Representation of the first dataset in A (black) and $\Phi_2^{(i)}$ (gray) coordinates. Right Panel: Representation of the second dataset, a simulation with slightly different initial population density, in A (black) and $\Phi_2^{(i)}$ (gray) coordinates. The coordinate $\Phi_2^{(i)}$ is a more useful coordinate than A, which may take on a range of values when the school is in the same collective state.
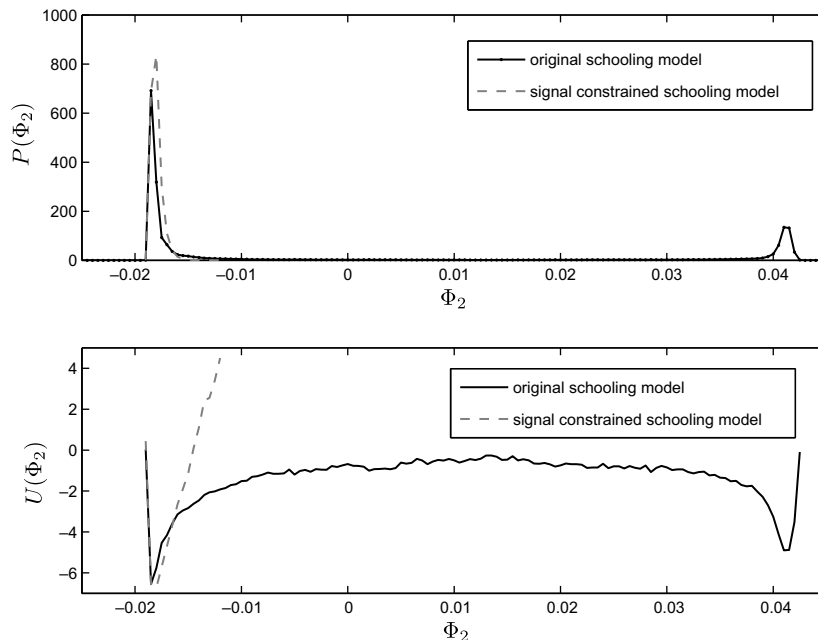

Fig. 5. Probability distributions and corresponding effective potentials for the original and the signal constrained schooling model with $\Delta r_o = 0.2$.

is used in Fig. 5, in which the probability distribution functions and corresponding effective potentials for the original and signal constrained schooling model are compared for $\Delta r_o = 0.2$. In each case, a database was formed from one hundred 10^4 step simulations, with the first 1000 transient steps discarded. As one can see from the figure, for $\Delta r_o = 0.2$, the original model has two metastable states, the stationary state at $\Phi_2 \approx -0.018$ and the mobile state at $\Phi_2 \approx 0.042$. The school exhibits stochasticity-induced switching between these states, spending more time in the stationary than in the mobile state on average. For this same parameter value, the signal constrained schooling model has only one stable state at $\Phi_2 = -0.018$, remaining in the stationary state for the entire duration of the simulations. For larger values of Δr_o, the signal con-

strained model does exhibit switching between the stationary and mobile state. It therefore appears that the signalling constraint prevents the mobile state from existing below a certain threshold of the parameter Δr_o. We will investigate the precise parametric dependencies in the next section.

Alternatively, one may construct an effective potential by assuming that the observable X obeys an effective Langevin equation, or equivalently its probability distribution $P(X)$ obeys an effective Fokker-Planck equation

$$\frac{\partial P(X,t)}{\partial t} = -\frac{\partial}{\partial X}\left[D^{(1)}(X)P(X,t)\right] + \frac{\partial^2}{\partial X^2}\left[D^{(2)}(X)P(X,t)\right]. \tag{13}$$
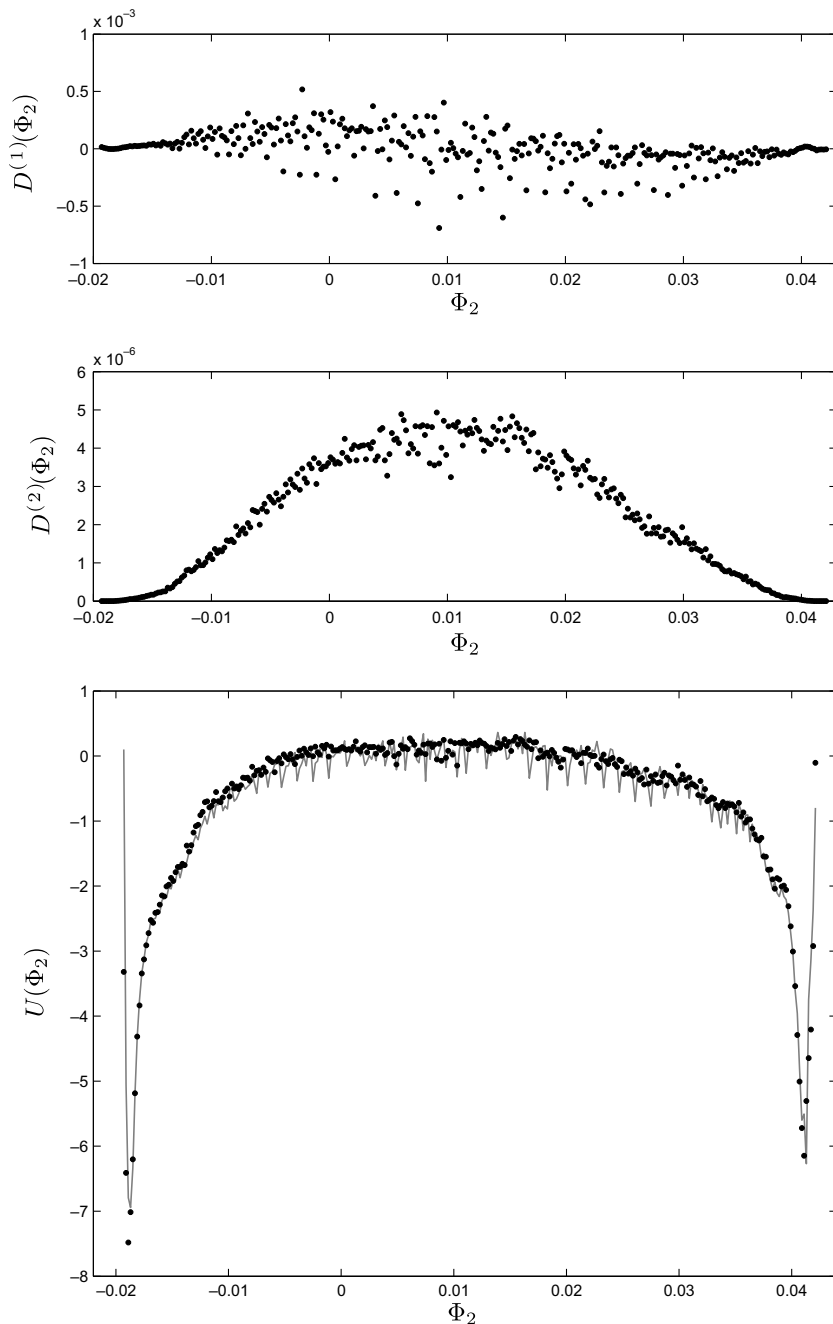

Fig. 6. Top: Drift $D^{(1)}(\Phi_2)$ and diffusion terms $D^{(2)}(\Phi_2)$ estimated from the simulation dataset. Bottom: Estimates of the effective potential, using $U(\Phi_2) = -\log(P(\Phi_2)) + \text{const.}$ (solid gray) and estimating the drift and diffusion terms and using Eq. (15) (black dots).

As described in [36], the drift $D^{(1)}(X)$ and diffusion term $D^{(2)}(X)$ are related to the short time evolution of the first two moments of an ensemble of replica simulations by

$$D^{(1)}(X_0) = \frac{\partial \langle X(t; X_0) \rangle}{\partial t}\bigg|_{t=0}, \qquad D^{(2)}(X_0) = \frac{1}{2}\frac{\partial \mathrm{Var}(t; X_0)}{\partial t}\bigg|_{t=0}, \qquad (14)$$

where $X(t; X_0)$ denotes a trajectory initialized at X_0 at $t = 0$, angular brackets denote ensemble averaging over different realizations of the trajectory, and Var denotes the variance of X for such an ensemble. Assuming $P(X) \sim \exp(-U(X))$ at steady state, it follows that the effective potential $U(X)$ satisfies

$$U(X) = \log(D^{(2)}(X)) - \int_{-\infty}^{X} \frac{D^{(1)}(X')}{D^{(2)}(X')}\,\mathrm{d}X' + \mathrm{const.} \qquad (15)$$

One may estimate the effective potential by compiling enough statistics from long-time simulation data to estimate the drift and diffusion terms using (14). More specifically, $X = \Phi_2$ is discretized over a grid of values in the range $[-0.019, 0.043]$ with a uniform grid spacing of size 10^{-3}. Then, for each X_0 over the grid, $D^{(1)}(X_0)$ and $D^{(2)}(X_0)$ are estimated as follows. Every appearance of X_0 in the database, within a certain error tolerance, is recorded. Its subsequent values are saved over a fixed time interval of 10 steps and the mean $\langle X(t; X_0) \rangle$ and variance $\mathrm{Var}(t; X_0)$ are computed by averaging over these segments. Finally, $D^{(1)}(X_0)$ (resp., $D^{(2)}(X_0)$) are estimated by computing the slope of the linear regression of $\langle X(t; X_0) \rangle$ (resp., $\mathrm{Var}(t; X_0)$). Once the drift and diffusion terms have been estimated, $U(X)$ may then be estimated by numerically approximating the integral in Eq. (15).

Fig. 6 shows the drift, diffusion, and effective potential as a function of $X = \Phi_2$, the latter obtained using both estimation approaches for the original schooling model with $\Delta r_o = 0.6$. The effective potential formed using Eq. (14) agrees very well with that obtained using the relation $U(X) = -\log(P(X)) + \mathrm{const}$, which supports our choice of Φ_2.

With $U(X)$ and $D^{(2)}(X)$ computed using the second approach, we may estimate the mean residence times in each well using Kramers theory. If $D^{(2)}(X)$ is relatively small, the average time T spent in a well located at $X = X_{\min}$ is approximated by [37]

$$T \approx \frac{2\pi \exp(\Delta U)}{\overline{D}\sqrt{-U''(X_{\min})U''(X_{\max})}}, \qquad (16)$$

where $X = X_{\max}$ is the location of the local maximum (saddle point) of the potential U, $X_{\min}$ is the location of the local minimum, $\overline{D} = \frac{1}{2}(D^{(2)}(X_{\max}) + D^{(2)}(X_{\min}))$, and $\Delta U = U(X_{\max}) - U(X_{\min})$.

For $\Delta r_o = 0.6$, the mean residence times were estimated to be $T = 850$ timesteps for the leftmost well and $T = 321$ for the well on the right. The second derivatives in Eq. (16) were estimated using a centered difference approximation. These estimated times compare well to the mean residence times observed directly from the simulation ensemble database, which gave times of approximately $T_1 = 1026$ and $T_2 = 507$ for $\Delta r_o = 0.6$. This lends further support that Φ_2 is an appropriate dynamic observable for the schooling model.

7. Coarse bifurcation diagrams

We investigate the dependencies of the schooling model on the parameter Δr_o, the width of the zone of orientation, by tracking the critical points of the corresponding effective potentials. As in deterministic bifurcation diagrams, we associate minima of the effective potential with stable fixed points and 1-D maxima (more generally, saddle points) with unstable fixed points. With this association, we may form a coarse bifurcation diagram by locating the critical points of the effective potential as the parameter Δr_o is varied.
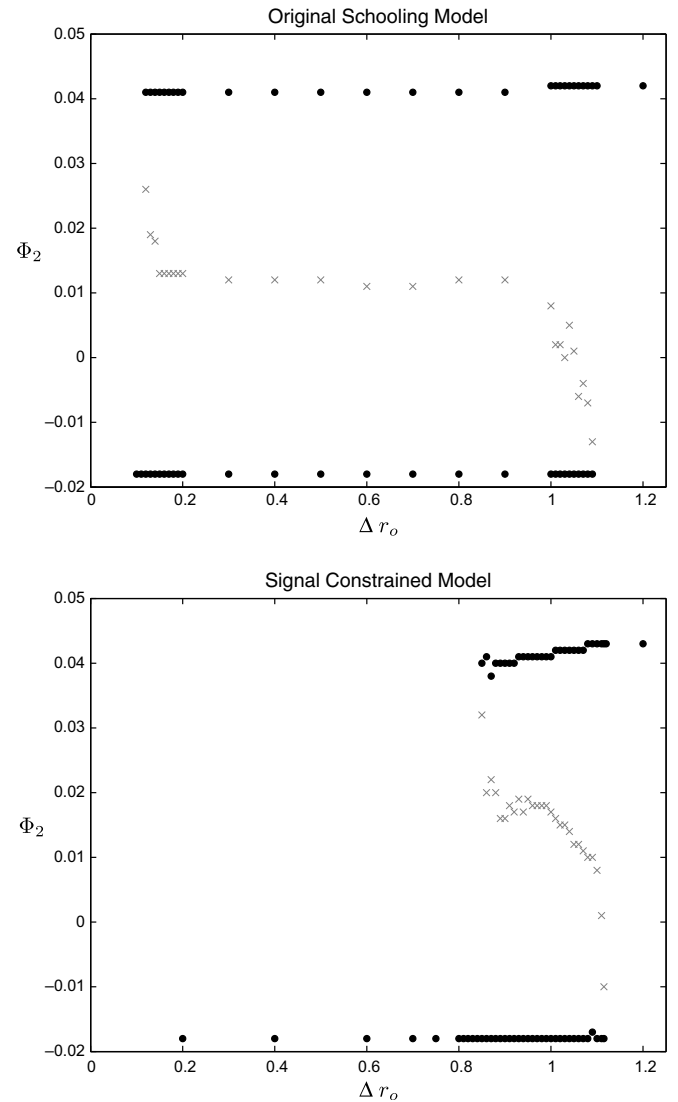

Fig. 7. Coarse bifurcation diagrams showing the critical points of the effective potential as Δr_o is varied. The minima of the effective potential correspond to the stable branch (black dots) and the maxima correspond to the unstable branch (gray x's). Top panel: original schooling model; Bottom panel: signal constrained schooling model.

As we discussed in Section 5, school fragmentation occurs with some probability in many of our simulations. Thus, some of the effective potentials (and associated probability distribution functions) have multiple valleys (peaks) for values of Δr_o within the bistable range. These metastable states are associated with the fragmentation of the group into non-coordinated subgroups and are typically quite small in comparison to the coordinated wells. To filter out such spurious states, we perform a quadratic fit of the effective potential between the stationary and mobile wells. This allows us to *estimate* the saddle point of the effective potential, and thus obtain a good approximation of the unstable branch of the bifurcation diagram. See Fig. 7 for bifurcation diagrams of both the original and signal constrained schooling model.

For the original schooling model, two saddle node bifurcations are found at $\Delta r_0 \approx 0.12$ and $\Delta r_0 \approx 1.1$ and the system is bistable for Δr_0 within this range. The diagram compares well qualitatively and quantitatively with the one constructed in [13] with the empirical observable A. For the signal constrained model, we also find two saddle node bifurcations, but they are located at $\Delta r_0 \approx 0.85$ and $\Delta r_0 \approx 1.2$. Thus, it seems that the signalling
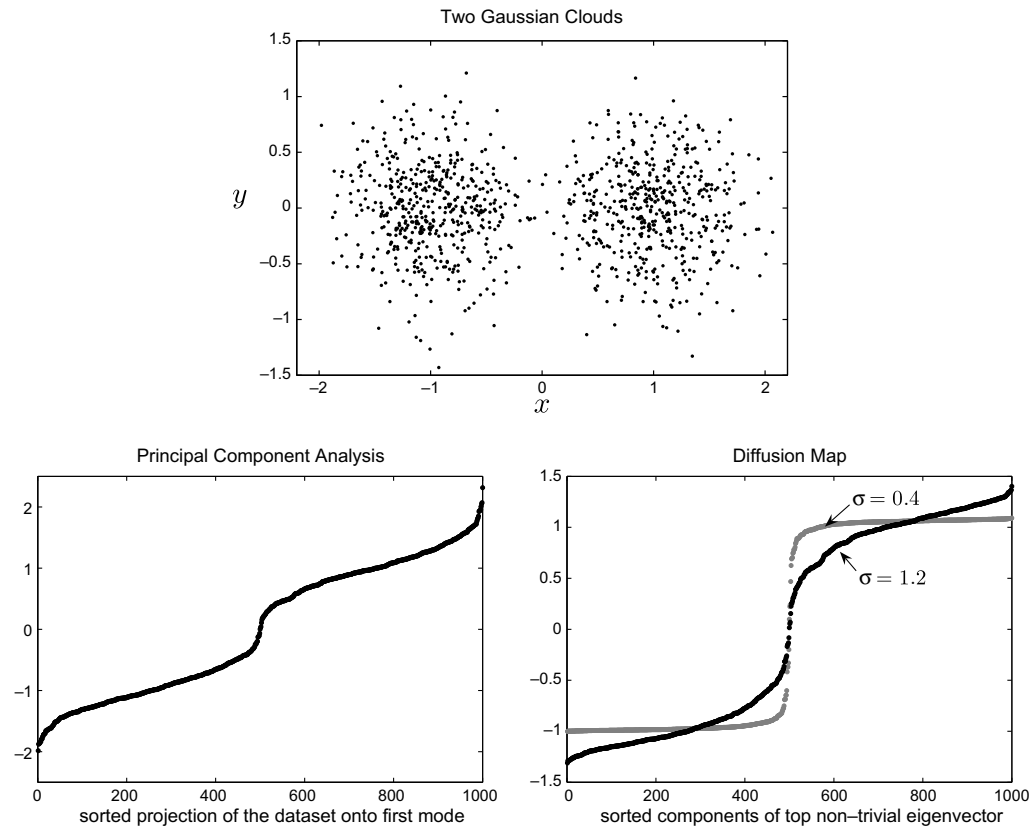
Fig. 8. (Top) Dataset sampled from two normal distributions centered at $(-1,0)$ and $(1,0)$ with standard deviation $\sigma_c = 0.4$ in each case. (Bottom left) Sorted projection of the dataset onto the first mode obtained using Principal Component Analysis. (Bottom right) Sorted components of the first non-trivial eigenvector obtained from the diffusion map procedure with $\sigma = 0.4$ (gray) and $\sigma = 1.2$ (black).

constraint effectively prevents the mobile state from existing below $\Delta r_o = 0.85$, and the parameter range for which the original model is bistable is effectively shortened.

We can rationalize the effect of the signalling constraint as follows. The parametric range of existence (and stability) of the stationary state is virtually the same for both models. This is not surprising since this state is driven by repulsion events, which are unaffected by the signalling constraint. On the other hand, a larger Δr_o is necessary to get sufficiently many interactions when the signalling constraint is present to 'hold together' the mobile state.

8. Conclusion

We studied the effects of a signalling constraint on an individual-based model of self-organizing group formation using a coarse analysis framework. This involved the selection of a coarse variable by defining a diffusion process on a graph constructed from a sample dataset formed from a representative stationary simulation. The eigenvectors of the graph Laplacian were used to construct 'diffusion-map' coordinates which provide a geometrically meaningful low-dimensional representation of the dataset. The first non-trivial (second principal) eigenvector provided a sufficient representation of the dataset, so we used it as a coarse observable. This facilitated the computation of coarse bifurcation diagrams, which showed that the signalling constraint reduces the region over which there is bistability between the stationary and mobile collective motion states. Overall, our results suggest that the diffusion map framework is a promising approach for understanding collective motion for fish schooling models.

Our approach in this paper complements the one used in [13]. The main difference in methodology is that [13] used the average

distance to nearest neighbor as a coarse variable to characterize the collective behavior of the school. This was shown to be a dynamically meaningful observable through computational experiments to test possible candidate observables. In this paper, we instead used an automated data-driven technique for generating the coarse variable. Although it is difficult to interpret this coarse variable physically, we were able to use it to construct effective potentials and calculate bifurcation behavior. Notably, the approach described in this paper overcomes the 'neutral stability' issue that arose for the coarse observable used in [13]. We also note that [13] developed a 'lifting' procedure which initializes the individual-based model with a particular value of the coarse variable and allowed more efficient population-level analysis. The need for lifting (and the associated difficulties) did not arise in the computations presented here.

The framework developed here provides a useful, computer-assisted approach for the analysis of emergent phenomena in individual-based models for collective motion. Most analysis of individual-based models in the field of group formation has relied on costly long-time simulations, which has limited the number of individuals that can be simulated as well as the types of analysis that can be realistically done [38]. This approach allows one to achieve a new level of understanding and quantification of biological self-organization by bridging individual-based modeling with coarse, population-level analysis. A challenge for extending this framework to two- or three-dimensional schools is the development of an appropriate measure for the distance between two schools, which perhaps would have to take into account the positions *and velocities* of all individuals. This would allow the computation of diffusion map coordinates which could aid in a similar analysis of stochasticity-induced switching between the milling and parallel motion states as was reported in Fig. 7 of [13].

Acknowledgements

Appendix. Comparison of diffusion maps and principal component analysis

The diffusion map approach can be thought of as a non-linear extension of principal component analysis (PCA) [22,32]. In PCA, analysis of a dataset is based on the assumption of linearity. A sample dataset is re-expressed through a linear transformation in terms of a new orthogonal basis which optimally captures the variance in the dataset. The first few modes provide a low-dimensional representation of the dataset. However, due to this linearity assumption, PCA may not always find an optimal (in terms of low-dimensionality) representation of the dataset. For example, consider as in Fig. 8, two Gaussian clouds in the plane drawn from normal distributions centered at $(-1,0)$ and $(1,0)$ with standard deviation $\sigma_c = 0.4$ in both cases. For this dataset, PCA finds the optimal basis to be $e_1 = [1,0]$ and $e_2 = [0,1]$. In Fig. 8, the projection of the dataset onto the first basis vector is plotted, which in this example is equivalent to plotting the x-coordinates of the datapoints. As one can see from the bottom left panel of the figure, the first modal coordinate does not give a sharp parametrization of the dataset which distinguishes between the two cloud clusters.

In contrast, using the diffusion map approach, with Gaussian kernel of a sufficiently small variance σ^2, we can capture the bimodal structure of the dataset with a single coordinate. In the bottom right panel of Fig. 8, the sorted components of the first non-trivial eigenvector obtained from the diffusion map procedure with $\sigma = 0.4$ and $\sigma = 1.2$ are plotted. The parameter σ controls the connection strength of the graph of the dataset. As one can see from the figure, for $\sigma = 1.2$ the parametrization of the dataset appears similar to that of PCA, while for $\sigma = 0.4$, the first non-trivial eigenvector is approximately constant in each cloud with a sharp transition between them. This is due to the fact that for σ sufficiently small, the two clouds are not directly connected in the graph of the dataset and are therefore quite far away in diffusion distance. Thus, if σ^2 is chosen to be of the same order as the variance σ_c^2 of the dataset, the diffusion map approach is able to capture the bimodal structure with a single coordinate.

References

[1] S. Camazine, J.L. Deneubourg, N.R. Franks, J. Sneyd, G. Theraulaz, E. Bonabeau, Self-Organization in Biological Systems, Princeton University Press, Princeton, 2003.

[2] P.B.S. Lissaman, C.A. Shollenberger, Formation flight of birds, Science 168 (1970) 1003.

[3] B.L. Partridge, The structure and function of fish schools, Sci. Am. 246 (1982) 90.

[4] A.R.E. Sinclair, M. Norton-Griffiths, Serengeti: Dynamics of an Ecosystem, University of Chicago, Chicago, 1979.

[5] B.P. Uvarov, Grasshoppers and Locusts, Imperial Bureau of Entomology, London, 1928.

[6] D.R. Martinez, E. Klinghammer, The behavior of the whale orcinus orca: a review of the literature, Z. Tierpsychol. 27 (1970) 828.

[7] D. Grünbaum, Schooling as a strategy for taxis in a noisy environment, Evol. Ecol. 12 (1998) 503.

[8] R.M. May, Flight formations in geese and other birds, Nature 282 (1979) 778.

[9] D. Wiehs, Hydrodynamics of fish schooling, Nature 241 (1973) 290.

[10] P.M. Driver, D.A. Humphries, Protean Behavior: The Biology of Unpredictability, Oxford University Press, Oxford, 1988.

[11] S.R.S.J. Neill, J.M. Cullen, Experiments on whether schooling by their prey affects the hunting behavior of cephalopods and fish predators, J. Zool. 172 (1974) 549.

[12] K.H. Koltes, Temporal patterns in three-dimensional structure and activity of schools of the Atlantic silverside Menidia menidia, Marine Biol. 78 (1984) 113.

[13] A. Kolpas, J. Moehlis, I.G. Kevrekidis, Coarse-grained analysis of stochasticity-induced switching between collective motion states, Proc. Natl. Acad. Sci. USA 104 (14) (2007) 5931.

[14] B.L. Partridge, T.J. Pitcher, The sensory basis of fish schools: relative roles of lateral line and vision, J. Comp. Physiol. 135 (1980) 315.

[15] S.J. Simpson, G.A. Sword, P.D. Lorch, I.D. Couzin, Cannibal crickets on a forced march for protein and salt, Proc. Natl. Acad. Sci. USA 103 (11) (2006) 4152.

[16] S.R. Witkin, The importance of directional sound radiation in avian vocalization, The Condor 79 (4) (1977) 490.

[17] J.A. Endler, Some general comments on the evolution and design of animal communication systems, Philos. Trans. R. Soc. London Ser. B 340 (1993) 215.

[18] P. Marler, Animal communication signals, Science 157 (1967) 769.

[19] R. Eftimie, G. de Vries, M.A. Lewis, Complex spatial group patterns result from different animal communication mechanisms, Proc. Natl. Acad. Sci. USA 104 (17) (2007) 6974.

[20] M. Belkin, P. Niyogi, Laplacian eigenmaps for dimensionality reduction and data representation, Neural Comput. 15 (2003) 1373.

[21] R.R. Coifman, S. Lafon, Diffusion maps, Appl. Comput. Harmon. Anal. 21 (2006) 5.

[22] I.T. Jolliffe, Principal Component Analysis, Springer-Verlag, New York, 1986.

[23] B. Nadler, S. Lafon, R.R. Coifman, I.G. Kevrekidis, Diffusion maps, spectral clustering and reaction coordinates of dynamical systems, Appl. Comput. Harmon. Anal. 21 (2006) 113.

[24] I. Aoki, A simulation study on the schooling mechanism in fish, Bull. Jap. Soc. Fish. 48 (1982) 1081.

[25] J. Buhl, D.J.T. Sumpter, I.D. Couzin, J.J. Hale, E. Despland, E.R. Miller, S.J. Simpson, From disorder to order in marching locusts, Nature 312 (2006) 1402.

[26] I.D. Couzin, J. Krause, R. James, G.D. Ruxton, N.R. Franks, Collective memory and spatial sorting in animal groups, J. Theor. Biol. 218 (2002) 1.

[27] A. Czirók, T. Vicsek, Collective motion, in: T. Vicsek (Ed.), Fluctuations and Scaling in Biology, Oxford University Press, Oxford, 2001, p. 177.

[28] T.A. Frewen, I.D. Couzin, A. Kolpas, J. Moehlis, R. Coifman, I.G. Kevrekidis, Coarse collective dynamics of animal groups, Phys. Rev. E Submitted for publication.

[29] B. Nadler, S. Lafon, R.R. Coifman, I.G. Kevrekidis, Diffusion maps, spectral clustering and eigenfunctions of Fokker-Planck operators, in: Y.W. et al. (Ed.), Advances in Neural Information Processing Systems, vol. 18, MIT Press, Cambridge, MA, 2005, pp. 955–962.

[30] R. Erban, T.A. Frewen, X. Wang, T.C. Elston, R. Coifman, B. Nadler, I.G. Kevrekidis, Variable-free exploration of stochastic models: a gene regulatory network example, J. Chem. Phys. 126 (2007) 155103.

[31] C.R. Laing, T.A. Frewen, I.G. Kevrekidis, Coarse-grained dynamics of an activity bump in a neural field model, Nonlinearity 20 (9) (2007) 2127.

[32] B. Schölkopf, A. Smola, K.R. Müller, Nonlinear component analysis as a kernel eigenvalue problem, Neural Comput. 10 (1998) 1299.

[33] C.D. Meyer, Matrix Analysis and Applied Linear Algebra, SIAM, Philadelphia, PA, 2000.

[34] C. Baker, The Numerical Treatment of Integral Equations, Clarendon Press, Oxford, 1977.

[35] S. Lafon, R.R. Coifman, Geometric harmonics: a novel tool for multiscale out-of-sample extension of empirical functions, Appl. Comput. Harmon. Anal. 21 (2006) 31.

[36] H. Risken, The Fokker–Planck equation: Methods of Solution and Applications, Springer-Verlag, Berlin, 1996.

[37] C. Gardiner, Handbook of Stochastic Methods, Springer-Verlag, Berlin, 2004.

[38] J.K. Parrish, S.V. Viscido, D. Grünbaum, Self-organized fish schools: an examination of emergent properties, Biol. Bull. 202 (2002) 296.